PAPER

Check for updates

Cancer cell membrane-camouflaged MOF nanoparticles for a potent dihydroartemisinin-based hepatocellular carcinoma therapy†

Yusha Xiao,‡[a] Wei Huang,‡[b] Daoming Zhu,[c] Quanxiong Wang,[a] Baiyang Chen,[a] Zhisu Liu,[a] Yang Wang [ID] *[b] and Quanyan Liu [ID] *[d]

Developing new drugs for cancer treatment remains a challenging task. Herein, cancer cell membrane biomimetic ferrous ion-doped metal–organic framework nanoparticles (ZIF-8 nanoparticles) combined with dihydroartemisinin (DHA) have been designed for targeted cancer treatment with low toxicity and side effects. The biomimetic nanomaterials (CDZs) have excellent homologous targeting ability and can accumulate in tumor tissues. In an acid tumor microenvironment, ferrous ions and DHA could be released with the degradation of materials. DHA, an ancient Chinese medicine, combines with ferrous ions to produce a powerful anti-tumor effect. In human liver cancer models, about 90.8% of tumor growth was suppressed. In addition, the nanomaterial has no obvious toxic and side effects *in vivo* and is a highly effective and low-toxicity anti-tumor drug with a strong clinical application value.

Introduction

Hepatocellular carcinoma (HCC) is the second leading cause of cancer-related death worldwide.[1] The existing treatments for HCC have low efficacy and suffer from systematic toxicity and side effects such as cardiotoxicity and myelosuppression. Thus, there exists an urgent need to develop more effective and targeted drug delivery systems for HCC.[2]

Dihydroartemisinin (DHA) is the derivative of artemisinin, also known as qinghaosu. In recent years, researchers have focused not only on the anti-malarial properties of DHA, but also on its anticancer properties.[3,4] DHA has an effect on the mitochondria-dependent apoptosis pathway and suppresses the activation of NF-κB, thus promoting tumor cell apoptosis;[5,6] it can also arrest the cell cycle and directly kill tumor cells mediated by Fe^{2+}.[7] When Fe^{2+} binds to DHA, the reductive scission of the peroxide bridge is induced and oxygen centered radicals are produced that can lead to the realignment of carbon centered radicals, thus inducing the toxicity of DHA.[8] Chen *et al.*

[a]*Department of General Surgery, Research Center of Digestive Diseases Zhongnan Hospital of Wuhan University, Wuhan, 430071, Hubei, P. R. China*

[b]*School of Chemistry and Chemical Engineering, Yangzhou University, Yangzhou, 225009, Jiangsu, P. R. China*

[c]*Key Laboratory of Artificial Micro- and Nano-Structures of Ministry of Education, School of Physics and Technology, Wuhan University, Wuhan, 430071, Hubei, P. R. China*

[d]*Department of General Surgery, General Hospital of Tianjin Medical University, Tianjin, 300052, China. E-mail: spsslqy@vip.126.com*

‡ Both authors contributed equally to this work.

created multifunctional mesoporous nanoparticles as pH-responsive Fe^{2+} reservoirs and artemisinin vehicles for the synergistic inhibition of tumor growth.[9] Liu *et al.* designed a dihydroartemisinin and transferrin dual-dressed nano-graphene oxide for a pH-triggered chemotherapy.[10] Wang *et al.* prepared $Fe_3O_4@C@MIL-100(Fe)$ nanoparticles for the magnetically guided delivery of DHA and Fe ions for enhanced cancer therapy.[11] However, low drug loading efficiency, poor biocompatibility, and lack of immune evasion ability may significantly hinder the therapeutic effect of DHA and exacerbate the side effects. Overall, the development of suitable drug carriers for DHA remains a challenge.

Metal–organic frameworks (MOFs), formed by various metal ion nodes coordinated to organic molecule linkers, have exhibited great potential as drug nanocarriers due to their high pore volume, large surface area, and easy modulation of pore sizes *via* the tuning of organic groups within the frameworks.[12–15] The zeolitic imidazolate framework (ZIF-8), in particular, is a non-toxic and biocompatible MOF consisting of zinc ions and 2-methyl imidazolate. ZIF-8 is pH-sensitive as it is very stable under physiological conditions but degradable in acidic solutions, making it a desirable drug delivery vehicle in the context of the tumor microenvironment.[16,17] When ZIF-8 was suspended in acid solution (pH 5.0–6.0), the coordination between the zinc and imidazolate ions dissociated, and the structure of ZIF-8 began to decompose quickly; however, it is exceptionally stable in water and aqueous sodium hydroxide.[15] Exploiting these properties, we believe that the ZIF-8 nanoparticles can be used for efficient loading and controlled release of DHA. After doping Fe^{2+} in ZIF-8, Fe^{2+} reacted with DHA under acidic solutions and generated radicals or carbon centered

radicals, resulting in DNA damage, mitochondrial depolarization, and apoptosis.[8]

In this study, we designed cancer cell membrane (collectively referred to as CMS) camouflaged, pH-sensitive, and ferrous ion doped ZIF-8 nanoparticles loaded with DHA (collectively referred to as CDZs) for enhanced hepatocellular carcinoma therapy with low toxicity and side effects (Scheme 1). Cancer cells show a variety of unique properties, such as limitless replicative potential and resistance to cell death,[18] especially the immune escaping and homologous binding capabilities, which depend on the surface membrane proteins of the cancer cells, and can well overcome the shortcomings of immune clearance and non-specific binding *in vivo*;[19] thus, the obtained cancer cell membrane-loaded particles (CDZs) could demonstrate immune escaping and homologous targeting abilities inherited from the source cancer cells. The biomimetic nanoparticle consisted of an inner core with ZIF-8 nanoparticles loaded with DHA

(collectively referred to as DZs) and an outer cancer cell membrane shell. The Fe^{2+} doped ZIF-8 nanoparticles were prepared by a simple method using methanol as the solvent.[20] This method yielded well dispersed ZIF-8 nanoparticles with a narrow particle size distribution of 90–110 nm that were highly stable against agglomeration. Benefiting from the excellent immune escape ability and homologous targeting ability of the cancer cell membranes, CDZs revealed strong tumor specificity both *in vitro* and *in vivo*. Due to the Warburg effect, the pH of the tumor tissues was slightly lower than that of normal tissues,[21] for example, the pH of liver cancer tissues and normal tissues was 6.5 and 7.4, respectively. When the nanodrug carrier entered the liver tumor tissues and was exposed to acidic conditions, the lysosome with lower pH (4.5–5.0) and endosome (5.0–5.5) will let the drug carrier make greater response, forcing DHA and Fe^{2+} to be quickly released from the core of DZs and produce large amounts of ROS, finally achieving
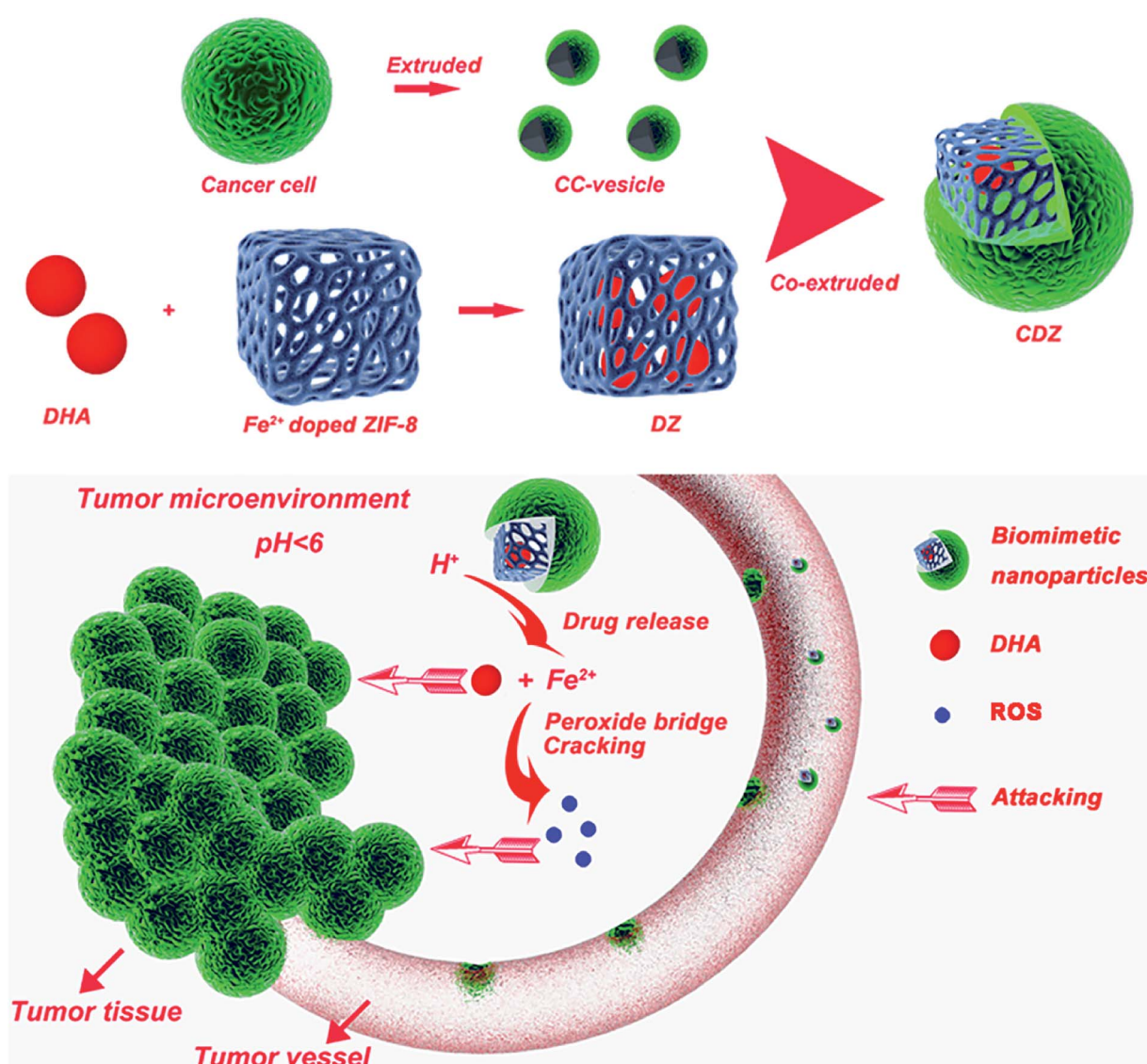
Scheme 1 Schematic illustration of cancer cell membrane-camouflaged pH-sensitive and ferrous ion-doped MOF nanoparticles loaded with dihydroartemisinin for enhanced hepatocellular carcinoma therapy with low toxicity and side effects.

the goal of stable targeted drug release. The released DHA and ROS showed potent anti-cancer effects both *in vitro* and *in vivo*. Remarkably, mice exhibited normal biochemical indicators before and after CDZ treatment, indicating superior biocompatibility and low side effects of the biomimetic nanoparticles. In all, we demonstrated that the cell membrane coated nanoplatform can be an effective HCC therapy with potentially minor side effects.

Experimental

Materials

All the reagents were used as purchased unless specified otherwise. Detailed information on the sources of chemicals is in the ESI.†

Cell and animal models

Hep G2 (G2) human hepatocellular carcinoma cell line, HCT116 human colorectal carcinoma cell line, MCF-7 human breast cancer cell line, the mouse leukocyte cell line (RAW264.7), human leukocyte cell line (U937), and L02 immortalized human hepatic cell line were purchased from the Cell Bank of Type Culture Collection (CBTCC, Chinese Academy of Sciences, Shanghai, China). The use of the above cell lines was approved by the Ethics Committee of Wuhan University. The cells were cultured in media supplemented with 10% FBS and 1% penicillin–streptomycin, and were incubated at 37 °C in a humidified incubator with 5% CO_2.

BALB/c nude mice (male, 4–6 weeks old, 18–22 g) were purchased from the Animal Center of the Chinese Academy of Medical Sciences (Beijing, China). All the animal procedures complied with the guidelines of the Institutional Animal Care and Use Committee at Wuhan University (Wuhan, Hubei, PR China), and the study was approved by the Ethics Committee of Wuhan University (Wuhan, Hubei, PR China).

Preparation and characterization of ferrous ion doped ZIF-8 nanoparticles

Ferrous ion doped ZIF-8 nanoparticles were obtained based on to the previous report after a minor modification.[22] The details can be found in the ESI.†

Preparation and characterization of CDZs

To obtain CDZs, an extrusion strategy was used.[23] The preparation and characterization of CDZs are described in detail in the ESI.†

In vitro immune evasion evaluation

U937 cells were seeded in confocal dishes at a density of 5×10^4 cells per dish and cultured for 12 h. Before the test, the growth medium was removed, then the cells were washed twice with PBS before adding the fresh growth media or media containing ICG labeled ZIF-8, DZs and CDZs at the concentration of 100 μg mL^{-1} into each dish. The cells were then incubated orderly for 4 h, washed with PBS several times, stained with DAPI, washed again, fixed with 4% PFA at room temperature, and imaged using CLSM under a 980 nm laser. Then, U937 cells were seeded in 12-well

plates at a density of 5×10^4 cells per well and cultured for 12 h. Before the test, the growth medium was removed. The cells were washed twice with PBS before adding ZIF-8, DZs, and CDZs into the fresh growth media at the concentration of 100 μg mL^{-1}. The cells were then incubated for 4 h and washed with PBS several times. To quantify the particle uptake by U937 cells, HNO_3 was added to dissolve the cells. The mixture samples were left at room temperature for 12 h, then heated at 70 °C to remove the acids, cooled down to room temperature, and resuspended in DI water for iron ion determination by using an inductively coupled plasma-atomic emission spectrometer (ICP-AES; IRIS Intrepid II XSP, Thermo Elemental, USA). Then, fixing the concentration at 100 μg mL^{-1} and changing the incubation time (2, 4, 6, 8, 10, and 12 h), the uptake was also measured by using ICP-AES.

Targeting ability of CDZs

To investigate the targeting ability of the CDZs, the G2, HCT116, and MCF-7 cells were seeded in confocal dishes and cultured for 24 h. Before the test, the cell medium was discarded. The cells were washed with PBS three times before the addition of cell medium or medium containing 100 μg mL^{-1} of various ICG-labeled nanoparticles (DZs and CDZs). The cells grown without the addition of any nanoparticles were used as the control. Then, the cells were orderly incubated for 2 h, washed with PBS, stained with DAPI, washed again, and observed by using CLSM. The fluorescent intensity of each group was calculated by a flow cytometer.

Cancer cell cellular uptake experiment

G2 cells were seeded in 12-well plates and cultured for 12 h. 100 μg of DZs and CDZs were added to the medium, and the cells grown without any particles were used as the control. Then, the cells were incubated for 4 h at 37 °C, 5% CO_2, and then washed with PBS three times. To quantify Fe uptake, the cells were lysed by adding 0.5 mL 1% Tween 80 to each well. The cell lysate from each well was then added to 1 mL nitric acid. The mixture was left at room temperature for 12 h, followed by annealing at 80 °C for 6 h to remove the acids. The sample was then resuspended with 1 mL DI water and the iron ion content of each sample was determined with ICP-AES. Then, in order to investigate the relationship between the uptake and the incubation time, we fixed the iron ion concentration of the nanoparticles at 100 μg mL^{-1} and changed the incubation time (*i.e.*, 6, 12, 18, and 24 h); the following steps were carried out as mentioned above.

Iron ion and DHA release experiments

The release of iron ions from CDZs was performed at 37 °C with suspensions (1 mL) containing 100 μg of nanoparticles at different pH values. Phosphate buffered saline (PBS) of pH = 7.4 and PBS of pH = 5.5 were employed as the release media to imitate normal blood/tissues and endosomal/lysosomal compartments of the tumor cells, respectively. At different time points, the samples were centrifuged to remove the nanoparticles. Finally, the supernatant was withdrawn to determine the concentration of the released iron ions using ICP-AES. The drug release experiment was performed at 37 °C. 1 mg of DZ and CDZ NPs was dispersed into 1 mL phosphate

buffer saline (PBS) solution of different pH values (5.5 and 7.4) and stirred under dark conditions. At a given time, the supernatant solution (5 mL) of each group was taken out by centrifugation and the amount of released DHA molecules was measured using a UV-Vis spectrophotometer at 210 nm.

In vitro biocompatibility and cytotoxicity assays

The biocompatibility was evaluated by performing CCK-8 assay and apoptosis detection assay. G2, RAW264.7, U937, and L02 cells were seeded in 96-well plates at a density of 5×10^3 cells per well and incubated for 24 h. Then, the cells were treated with CZs at different concentrations (0.05, 0.10, 0.20, 0.50, 1.00, and 2.00 mg mL^{-1}). At the end of the incubation, 5 mg mL^{-1} CCK-8 PBS solution was added and the plate was incubated for another 4 h. Finally, the absorbance values of the cells were determined by using a microplate reader (Emax Precision, USA) at 450 nm. The background absorbance of the well plate was measured and subtracted. The cytotoxicity was calculated by dividing the optical density (OD) values of the treated groups (T) by the OD values of the control (C) ($T/C \times 100\%$).

For the apoptosis detection assay, G2 cells were first seeded into a 96-well plate with a density of 5×10^3 cells per well and cultured for 12 h. The cells were treated with different concentrations (0.10, 0.50, 1.00, and 2.00 mg mL^{-1}) of CZs and maintained for 24 h at 37 °C under 5% CO$_2$ in an incubator. At the end of the incubation, the Alexa Fluor 488 Annexin V/PI Cell Apoptosis Kit was used to detect and quantify the apoptosis by BD Accuri C6 flow cytometer (USA).

The cytotoxicity was measured by the CCK-8 assay, G2 cells were seeded in 96-well plates at a density of 5×10^3 cells per well and incubated for 24 h. Afterwards, the cells were treated with DHA, DZs, and CDZs at the DHA concentration of 30 μg mL^{-1}. At the end of the incubation, 5 mg mL^{-1} CCK-8 PBS solution was added and the plate was incubated for another 4 h. Finally, the absorbance values of the cells were determined by using a microplate reader (Emax Precision, USA) at 450 nm. The background absorbance of the well plate was measured and subtracted. The cytotoxicity was calculated by dividing the optical density (OD) values of the treated groups (T) by the OD values of the control (C) ($T/C \times 100\%$).

To further evaluation of the cytotoxicity of CDZs, G2 cells were seeded in 96-well plates at a density of 5×10^3 cells per well and incubated for 24 h. Then, the cells were incubated with PBS, DHA, DZs, and CDZs at the DHA concentration of 30 μg mL^{-1} for 24 h. Afterwards, the cells were stained with fluorescein diacetate (FDA) and observed under a fluorescence microscope (IX81, Olympus, Japan).

ROS levels and mitochondrial membrane potential (MMP) detection

For the determination of ROS levels *via* fluorescent imaging, HepG2 cells were co-incubated with four different groups for 6 h: control group, DHA groups (100 μg mL^{-1}), DZs (100 μg mL^{-1}), and CDZs groups (100 μg mL^{-1}), respectively. Then, the fluorescent dye, DCFH-DA (10 μmol L^{-1}), was added and co-incubated for 50 min at 37 °C. The ROS level was determined by the fluorescence
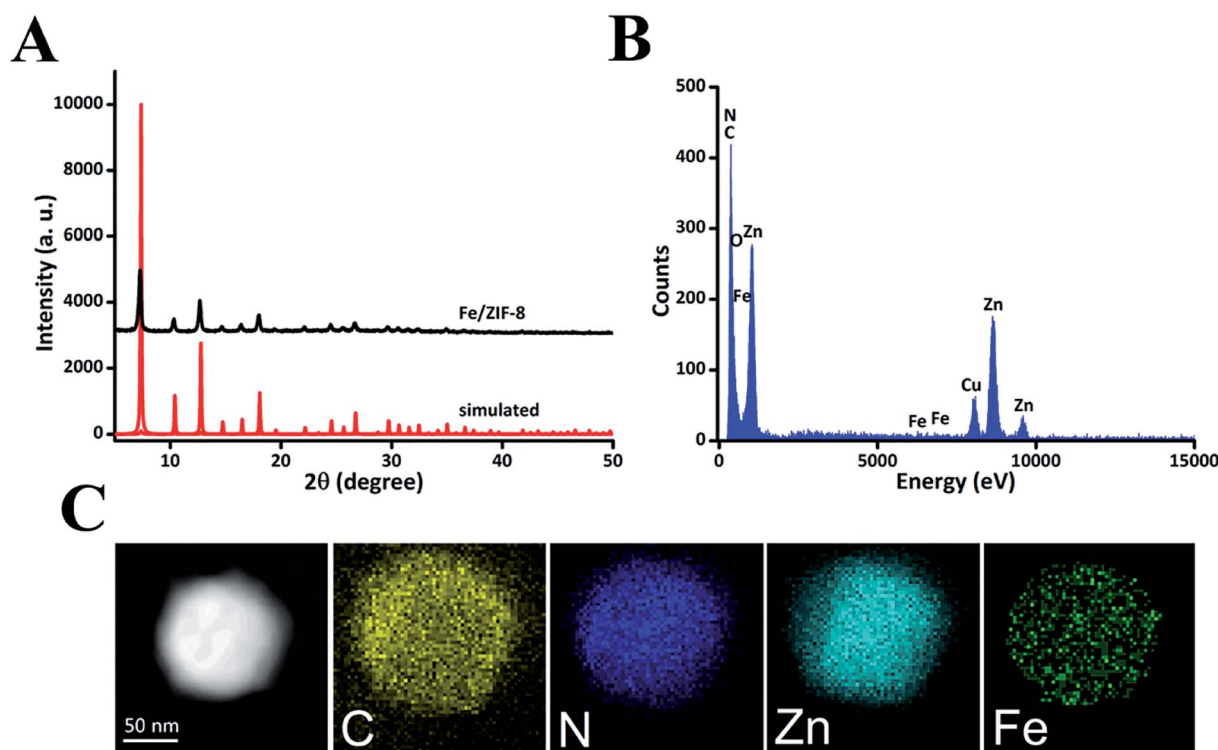

Fig. 1 Characterization of ZIF-8. (A) The powder X-ray diffraction pattern of Fe/ZIF-8. (B) The energy dispersive X-ray elements of Fe/ZIF-8. (C) The energy dispersive X-ray elemental mapping images of Fe/ZIF-8.

microscope (IX81, Olympus, Japan). The fluorescence intensity was determined by flow cytometry. For the JC-1 assay, the cells were co-incubated with different groups for 6 h: control group, DHA groups (100 μg mL^{-1}), DZs (100 μg mL^{-1}), and CDZs groups (100 μg mL^{-1}), respectively. The cells were stained with JC-1 for 30 min before washing with PBS. Then, the mitochondrial damage/disruption was detected by the fluorescence microscope (IX81, Olympus, Japan).

In vivo and ex vivo imaging

HepG2 cells (5 × 10^6 cells for each mouse) were subcutaneously injected into the flanks of 5 week BALB/c-nu mice to construct HepG2 tumor-bearing mice for the subsequent studies. The

imaging studies were performed when tumors reached ∼100 mm^3. We intravenously (i.v.) injected saline, ICG loaded DZs, and ICG loaded CDZs (100 μL, 100 μg mL^{-1} ICG) into the mice (n = 5). Then, 24 h after the injection, the acquired fluorescent images were taken on a vivo imaging system (IVIS Lumina XRMS Series III, USA) by 700 nm excitation wavelength. The mice after injection at 24 h were sacrificed and the organs including heart, liver, spleen, lung, kidneys, and tumor were collected for imaging and analysis.

Biodistribution analysis

For biodistribution assay, 100 μL free DHA, DZs, and CDZs at the dose of 1 mg mL^{-1} DHA was intravenously injected into the
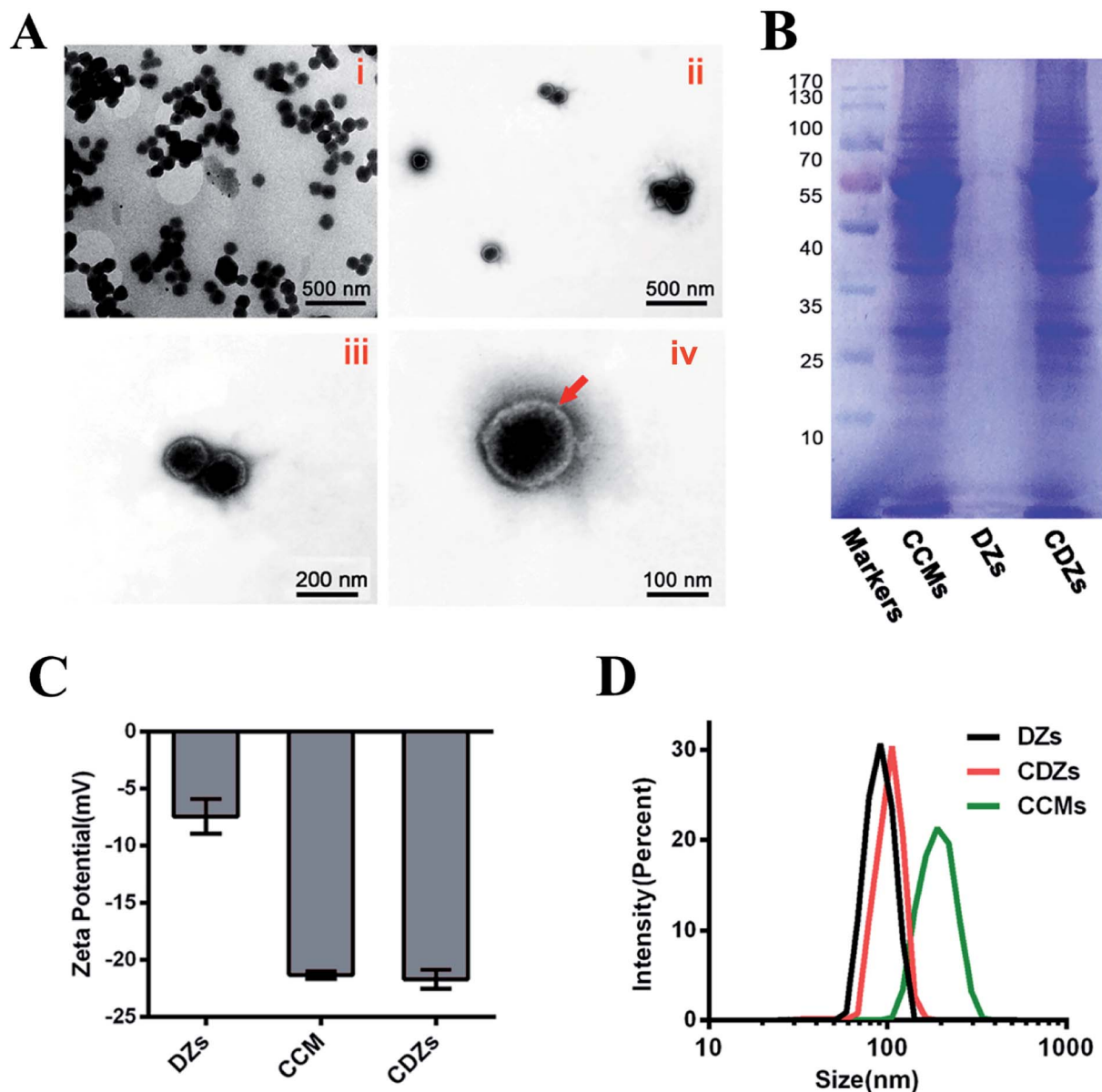

Fig. 2 Characterizations of CDZs. (A) TEM images of Fe/ZIF-8 nanoparticles (i) and CDZs (ii–iv) with different magnifications. The red arrow points to the cell membrane coating. (B) SDS-PAGE protein identification images of the cancer cell membranes (CCMs), DZs, and CDZs. (C) Zeta potential and (D) hydrodynamic diameter measurements of DZs, CCMS and CDZs (n = 3).

mice ($n = 5$) when the tumor size reached about 100 mm³. The mice were sacrificed at 24 h post-injection to extract various tissues including the heart, liver, spleen, lung, kidney, and tumor. In order to determine the contents of DHA, the tissues were further homogenized. 2.5 mL methanol was added to extract the DHA. The concentration of DHA was then determined using fluorescence spectroscopy.

In vivo anti-tumor tests

For the anti-tumor tests, when the tumor volume grew to about 100 mm³ after the injection, the mice were randomly assigned to five groups ($n = 5$) and intravenously injected with saline, CZs, DHA, DZs, and CDZs (100 μL, 1 mg mL⁻¹ of DHA and 1.4 mg L⁻¹ Fe/ZIF-8) every 3 d. The animal weight and tumor volume were measured every 3 d until the test ended. Tumor volume (V) was calculated using the formula: $V = (L \times W \times W)/2$ (L: the longest diameter of tumor and W: the shortest diameter perpendicular to the length). All the mice were photographed and euthanized, then the tumors were embedded in paraffin and subjected to the fluorescence TUNEL assay to measure the intratumoral late apoptosis.

In vivo toxicity assessment

The male BALB/c nude mice (18–22 g) were intravenously injected with saline, CZs, DHA, DZs, and CDZs (100 μL, 1 mg mL⁻¹ of DHA and 1.4 mg mL⁻¹ Fe/ZIF-8) every 3 d four times. All the mice were euthanized on the 19ᵗʰ day after the initial injection and the heart, liver, spleen, lung, and kidney were harvested. The obtained tissues were fixed in formalin for the next paraffin sectioning and hematoxylin and eosin (H&E) assays to evaluate the histopathologic toxicity of the typical tissues. The blood samples of the mice were also collected for the blood test. The blood parameters from the control and the treated mice were detected by using a blood automatic biochemical analyzer (Chemray, Rayto, China).

Statistical analysis

Data analyses were conducted using the GraphPad Prism 6.0 software. Statistical analysis was performed by using Student's t test. All the results were expressed as mean ± standard error unless otherwise noted. The difference between the two groups was considered statistically significant for *$p < 0.05$ and very significant for **$p < 0.01$.
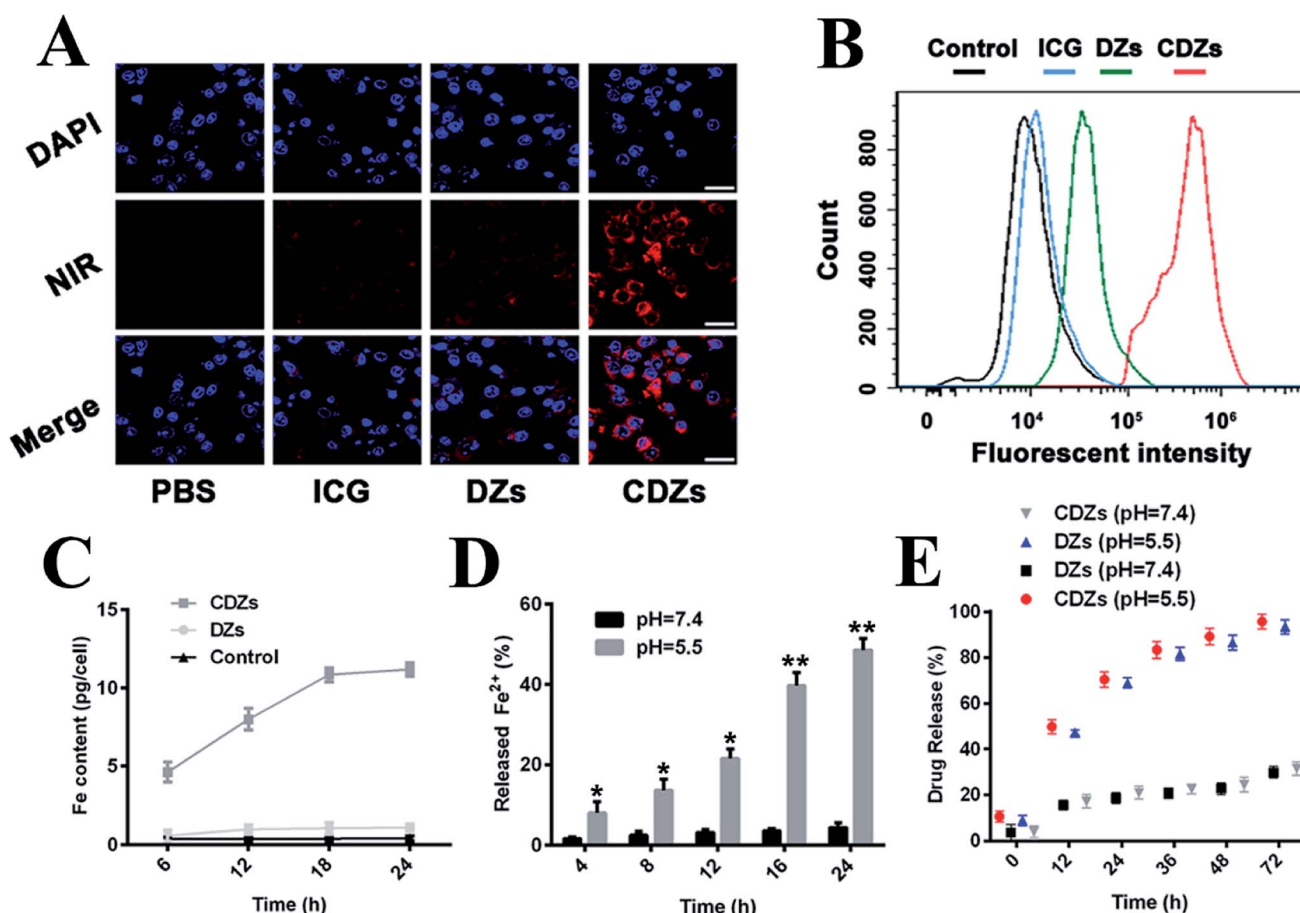

Fig. 3 Targeting ability and pH-sensitive drug release of CDZs. (A) CLSM photos of Hep G2 cancer cells after incubation with various ICG-labelled nanoparticles. Scale bar = 20 μm. (B) Flow cytometric analysis of mean fluorescent intensity in Hep G2 cells incubated with different formulations for 2 h. (C) Cellular uptake of different nanoparticles on Hep G2 cells after different incubation times ($n = 3$). (D) Release of Fe²⁺ ions from CDZs NPs in buffer solutions at pH 7.4 and 5.5 ($n = 3$). (E) In vitro release profiles of DHA from DZs and CDZs at different pH values ($n = 3$). Statistical significance: *$p < 0.05$ and **$p < 0.01$.

Results and discussion

Preparation and characterization

ZIF-8 is composed of dodecahedral crystal structure and each Zn^{2+} connects four imidazolate (im^-) ligands to form neutral frameworks. The introduction of Fe^{2+} in the crystal lattice results in a weak slowing down of the kinetics of ZIF-8 particle precipitation; each Zn^{2+} and Fe^{2+} combined with four imidazolate (im^-) ligands to form the framework under the addition of Fe^{2+} and Zn^{2+}. The powder X-ray diffraction (XRD) pattern of Fe/ZIF-8 was similar to that of simulated ZIF-8 (Fig. 1A), suggesting that highly crystalline structures were formed.[24] The energy dispersive X-ray (EDS) elements of Fe/ZIF-8 consisted of C, N, O, Zn, and a small amount of Fe (Fig. 1B). As shown in Fig. 1C, the elemental mapping analyses clearly exhibited the elemental distribution in the Fe/ZIF-8 nanostructure. It was obvious that the C, N, Zn, and Fe elements are uniformly distributed but Fe has a relatively low density. The X-

ray photoelectron spectroscopic (XPS) measurements were performed to confirm the surface elemental constitution in Fe/ZIF-8. The full survey of Fe/ZIF-8 (Fig. S1A†) showed the peaks of C 1s, N 1s, O 1s, Zn 2p, and Fe 2p, which further demonstrated the elemental composition of Fe/ZIF-8. The contents of the ions in the hybrid nanoparticles were 55.68% for C 1s, 27.14% for N 1s, O 1s (5.61%), Zn 2p (10.32%), and Fe 2p (1.25%). Fig. S1B† displayed the high resolution XPS spectra of Fe 2p in Fe/ZIF-8, the peaks at 724.8 eV, 723.0 eV, 713.9 eV, and 710.2 eV could be assigned to Fe(III) $2p_{1/2}$, Fe(II) $2p_{1/2}$, Fe(III) $2p_{3/2}$, and Fe(II) $2p_{3/2}$, respectively, besides, the satellite peak at 719.6 eV. This revealed that Fe(III) and Fe(II) coexist in Fe/ZIF-8. Fig. S2† showed the drug loading content (DLC) and drug loading efficiency (DLE), which were evaluated by high-performance liquid chromatography (HPLC) and calculated by the specified formula. The DLC and DLE of DZs were 42.2 ± 3.3% and 96.2 ± 3.6%, respectively, indicating DZs as a superior nanocarrier for drug delivery when compared to traditional
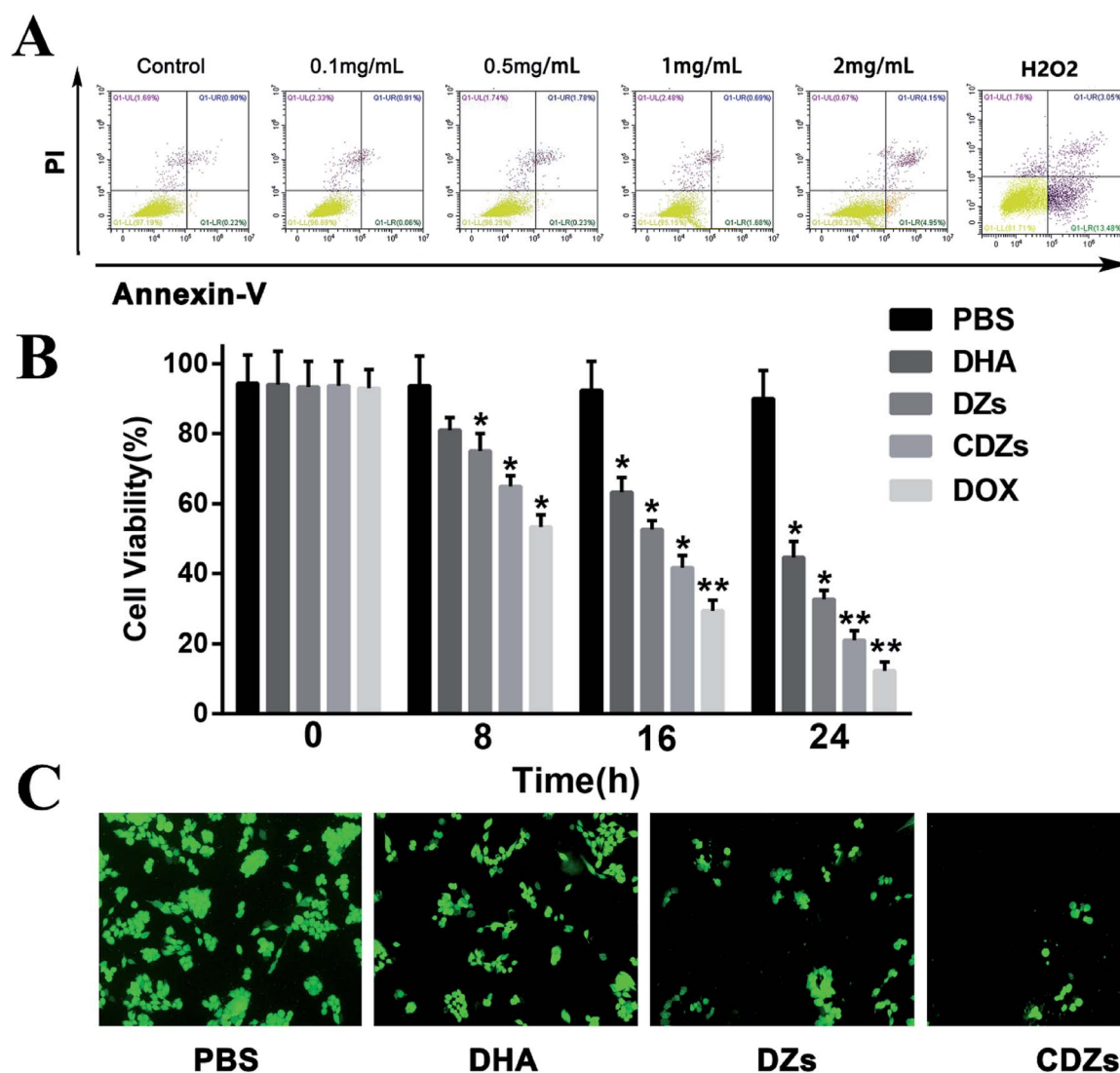

Fig. 4 *In vitro* biocompatibility and cytotoxicity assays. (A) Flow cytometry analysis of G2 cells after incubation with CZs at different concentrations. (B) Viability of G2 cancer cells after various treatments ($n = 3$). (C) Live cell staining of G2 cancer cells after various treatments. Scale bar = 50 μm. Statistical significance: *$p < 0.05$ and **$p < 0.01$.

systems.[11] From the N_2 sorption of Fe/ZIF-8 and Fe/ZIF-8 loaded DHA (Table S1†), the BET surface area of Fe/ZIF-8 is 1327 $m^2 g^{-1}$, the total pore volume and pore size are 0.637 $m^3 g^{-1}$ and 1.2 nm, respectively. After loading DHA, the BET surface area, total pore volume, and pore size were significantly reduced to 987 $m^2 g^{-1}$, 0.231 $m^3 g^{-1}$, and 0.5 nm, respectively, demonstrating that DHA was encapsulated in Fe/ZIF-8.

Transmission electron microscopy (TEM) was employed to characterize the morphology of DZs and CDZs. In Fig. 2A, a white film is shown to cover the DZ surface, making CDZs appear larger than DZs and demonstrating the successful coating of the DZs by the cell membranes. As shown in Fig. 2C, the zeta-potential of CDZs was −22.3 mV, which was close to that of CMSs (−21.6 mV) but much lower than that of DZs (−7.4 mV). The analysis of hydrodynamic size distribution (Fig. 2D) revealed that the average hydrodynamic diameter of DZs increased by 18 nm after being coated with CMSs. The particle size and zeta-potential both suggested the successful coating of cell membranes onto the nanoparticles. The prepared CDZs can be kept stable for 15 days in FBS or PBS solutions, ensuring its reliability for subsequent experiments (Fig. S3†). In the protein content assay (SDS-PAGE), no protein was observed in the DZ group while the CMS and CDZ groups exhibited similar protein expression levels, indicating successful translocation of the cell membrane onto DZs (Fig. 2B).

Targeting ability and pH-sensitive drug release of CDZs

The homologous targeting ability of the cancer cell membranes has been studied extensively in recent years.[25] Herein, confocal laser scanning microscopy (CLSM) was used to visually assess the targeting of hep G2 cells and other cancer cells by colocalization. As expected, the CDZ treatment group exhibited bright green fluorescence and higher fluorescent intensity than the other groups (Fig. 3A and B). This directly demonstrated the specific cancer targeting ability of CDZs and suggested the successful coating of the cell membranes. As shown in Fig. S5,† the CDZs prepared by hep G2 cell membrane also showed relatively poor targeting ability compared to other tumor cells (MCF-7 and HCT116), also proving its homologous targeting ability. To further verify the targeting capability of CDZs, phagocytosis was measured at different time points. As shown in Fig. 3C, CDZs had the highest cell phagocytosis compared with DZs and the control group, which was consistent with the results of confocal images, indicating good tumor targeting of CDZs.

The pH-sensitivity of CDZs was investigated by observing Fe^{2+} and DHA release under different pH conditions *in vitro*. There was a monotonic increase in the amount of Fe^{2+} released at pH 5.5 with nearly 50% of Fe^{2+} released after 24 h; significantly lower release was observed in a neutral environment (pH = 7.4) (Fig. 3D). This result indicates that the ZIF-8 nanoparticles can be stimulated by hydrogen ions and cause the release of the doped ferrous ions.[26] In Fig. 3E, we observed a similar behavior in the release of DHA in both CDZ and DZ groups with over 60% release at pH 5.5 compared to only 25% at pH 7.4, indicating the stability of CDZs in neutral pH physiological conditions. DHA release was significantly enhanced in acidic environment, which could be explained by the dissolution of CDZs and diffusion through the MOFs.[27,28]
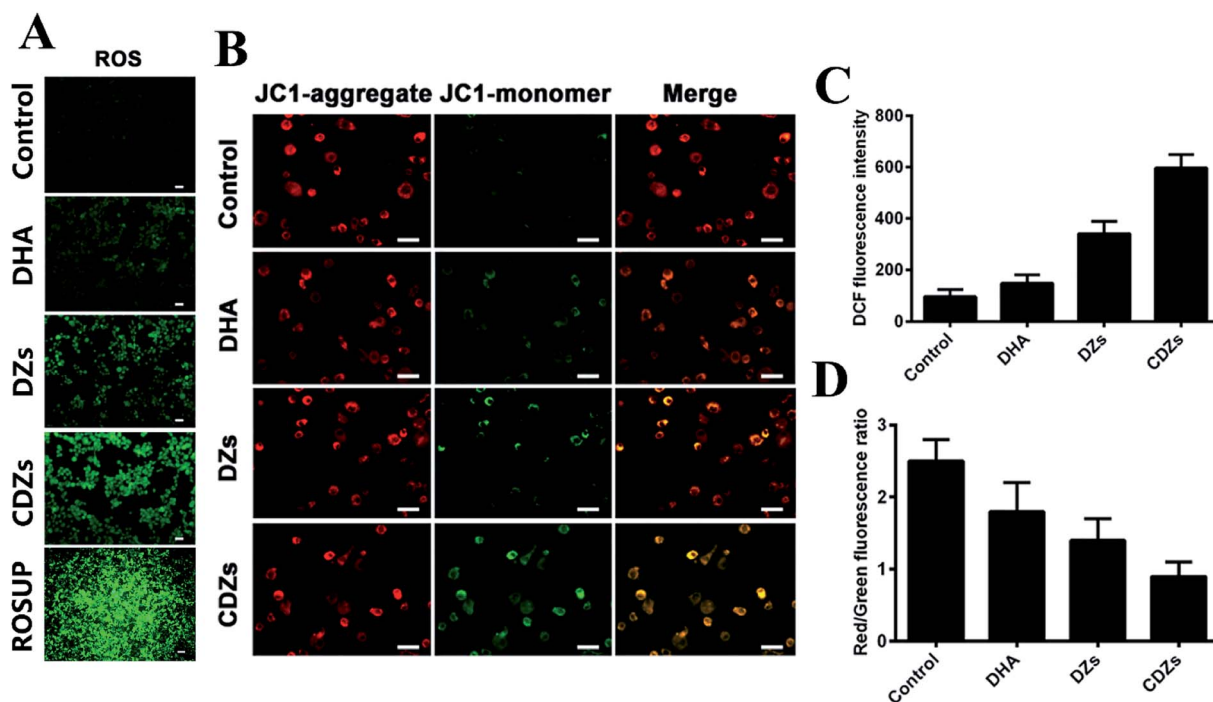

Fig. 5 ROS production in living cells was detected by reactive oxygen fluorescence probe DCFH-DA. (A) ROS levels and (B) mitochondrial membrane potential (MMP) measured by JC-1 staining of Hep G2 cells after being co-incubated at four groups for 6 h. (C) The fluorescence intensity of ROS levels ($n = 3$). (D) The fluorescence ratio of red JC-aggregate *vs.* green JC-monomer. ($n = 3$). Statistical significance: *$p < 0.05$ and **$p < 0.01$. Scale bar = 20 μm.

The immune avoidance ability of CDZs

We also studied the immune avoidance ability of CDZs. As shown in Fig. S6,† when CDZs were co-cultured with human leukocyte cell line U937 cells, the white blood cells showed poor phagocytic ability compared to the CDZs, the fluorescence in the cells was the weakest, and the detected iron was the lowest. However, they had strong phagocytic ability compared to pure ZIF-8 or DZs, indicating that the nanoparticles possessed immune escape ability after being coated with the tumor cell membrane.

In vitro biocompatibility and cytotoxicity assays

The biocompatibility of the cancer cell membrane coated Fe/ZIF-8 nanoparticles (CZs) was evaluated by CCK-8 assay and apoptosis assay. Fig. 4A and S4† show the viability of cells incubated with CZs at different concentrations. Even at a concentration of 2 mg mL^{-1}, the cell survival rate of both normal cells and tumor cells remained above 90%, suggesting good biocompatibility of CZs.

To evaluate the therapeutic cytotoxicity of CDZs, we used the counting kit-8 (CCK-8) assay to investigate the viability of hep G2 cells under CDZ treatment. In Fig. 4B, it can be seen that hep G2 cells treated with CDZs showed significant cell death (approximately 90%) when compared to other groups likely aided by specific targeting actions; doxorubicin (DOX) is an anthracycline antibiotic with anti-tumor activity, which is widely used in a variety of cancer treatments, so we chose DOX as a positive control for the cytotoxicity assay. Hep G2 cells treated with CZs exhibited the least cell death, indicating good biocompatibility and low toxicity of the nanoparticles. Both the DZs and DHA groups exhibited cytotoxicity with DZs being slightly more effective, indicating a synergy between Fe^{2+} and DHA. For further confirmation, fluorescein diacetate (FDA) staining was used to stain the live cells. In Fig. 4C, we saw that CDZs resulted in the least number of live cells followed by DZs and DHA. This showed that DHA had potent anti-cancer properties when used in conjunction with Fe^{2+} and the overall effect can be enhanced when they are applied in a targeted platform such as the CDZs.

ROS production

ROS production in living cells was detected by reactive oxygen fluorescence probe DCFH-DA. As shown in Fig. 5A and C, CDZs showed stronger DCF fluorescence than other groups, indicating that CDZs had a strong ability of reactive oxygen generation, which was consistent with the treatment results *in vitro*. In addition, excessive oxidative stress can also produce mitochondrial dysfunction. Therefore, we also measured changes in the mitochondrial membrane potential. We used a mitochondrial membrane potential (MMP) probe, JC1. Fluorescent red JC-aggregates were produced by JC-1 that gathered in the mitochondria. For damaged mitochondria, the MMP decreased
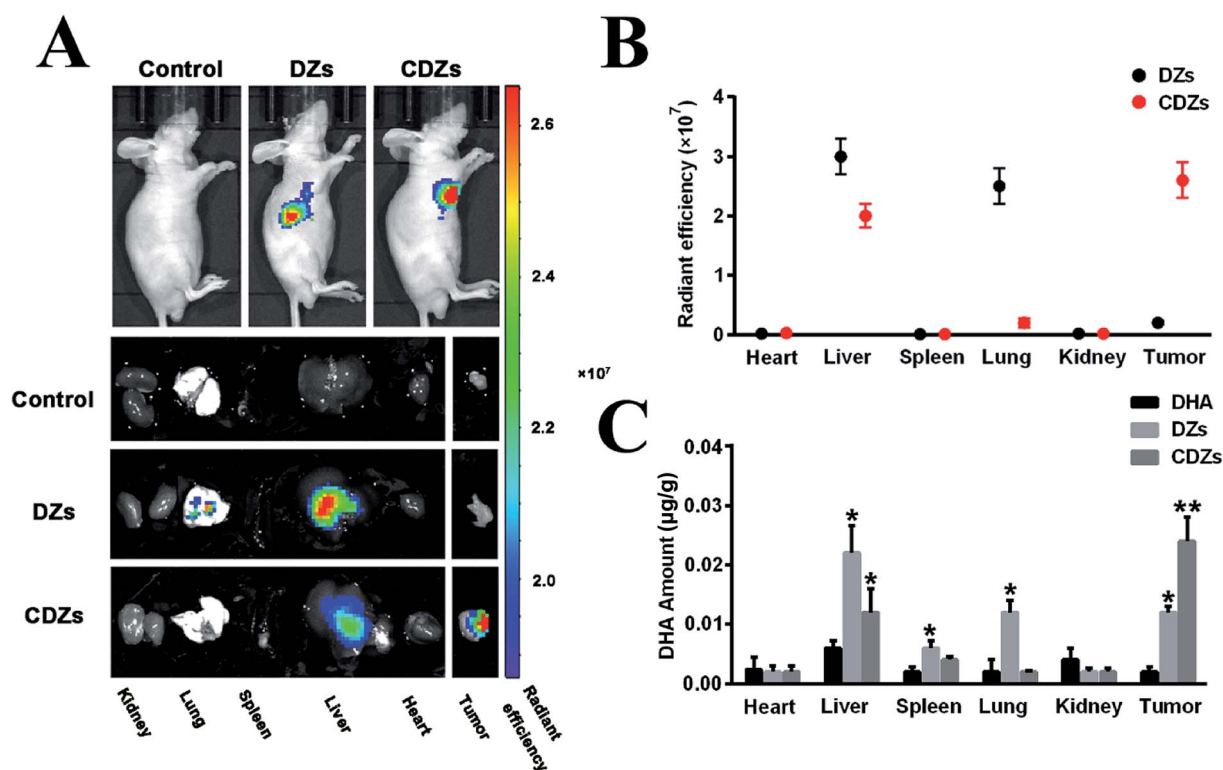

Fig. 6 NIR fluorescent (FL) images of major organs and nude mice bearing hepG2 tumors after intravenous injection of saline, ICG loaded DZs, or ICG loaded CDZs at 24 h. (A) Radiant efficiency of ICG loaded nanoparticles in major organs and cancer tissues at 24 h. The data are shown as mean ± SD (*n* = 5). (B) Quantitative *in vivo* biodistribution analysis of DHA in different formulations at 24 h after intravenous injection in nude mice bearing hep G2 tumors. The data are shown as mean ± SD (*n* = 5). (C) Quantitative *in vivo* biodistribution analysis of DHA after injection of different nanoparticles. Statistical significance: **p* < 0.05 and ***p* < 0.01.

due to fluorescent green JC-monomer generation by re-dispersion of red JC-aggregates in the cytoplasm.[29] As shown in Fig. 5B and D, the CDZs group had more green JC-monomer than the other groups and the ratio of JC-aggregate to JC monomer was smaller, indicating that the cell mitochondria were significantly damaged. In conclusion, the CDZs group had more active oxygen generation capacity.

In vivo tumor targeting ability

In vivo tumor targeting ability of CDZs was verified by vivo imaging and drug distribution experiments. The same amount of NIR fluorescent dyes (ICG) marked with different formulations was intravenously injected into tumor-burdened nude mice *in vivo*. Then, 24 h after injection, the mice were anesthetized for *in vivo* and *in vitro* organ imaging and analysis, using a live imaging equipment. As shown in Fig. 6A and B, CDZs in the tumor site had high fluorescence signal (about 2.6×10^7 for the radiation efficiency), while the DZs group showed weak fluorescence signal (radiation efficiency is about 0.5×10^7); the DZs had an obvious fluorescence signal in the liver and lungs, while CDZs in the liver and lungs showed an obvious weak fluorescence signal. This phenomenon was further confirmed by organ imaging. CDZs had good tumor targeting ability, abundant accumulation in the

tumor site, and takes less for the body to clear; this was all thanks to the homologous targeting ability and good immune evasion ability of the cancer cell membranes of the CDZs. Then, we studied the distribution of DHA after injection of different nanoparticles in the body (Fig. 6C). For pure DHA, very little drug accumulation in the main organs or tumor was observed, which was due to the rapid drug removal. For the DZs and CDZs groups, DZs showed high accumulation in the liver and lung, and a certain accumulation in the tumor site. In the CDZs group, DHA had high accumulation in the tumor site, while the accumulation in the liver and lungs was significantly reduced. DZs had no active targeting ability, so it can only accumulate in the tumor site passively and most of it was swallowed by the immune system. CDZs had active tumor targeting and immune evasion, so there was a lot of DHA in the tumor site but less in other parts. This is also consistent with the results of live imaging.

In vivo anti-tumor tests

The *in vivo* anti-cancer effects were evaluated in a subcutaneous tumor mouse model. In Fig. 7A, we saw that the tumors in both saline and CZ without DHA treatment groups displayed similarly uninhibited growth behavior. On the contrary, DZ treatment resulted in 56.9% reduction in the tumor volume, demonstrating
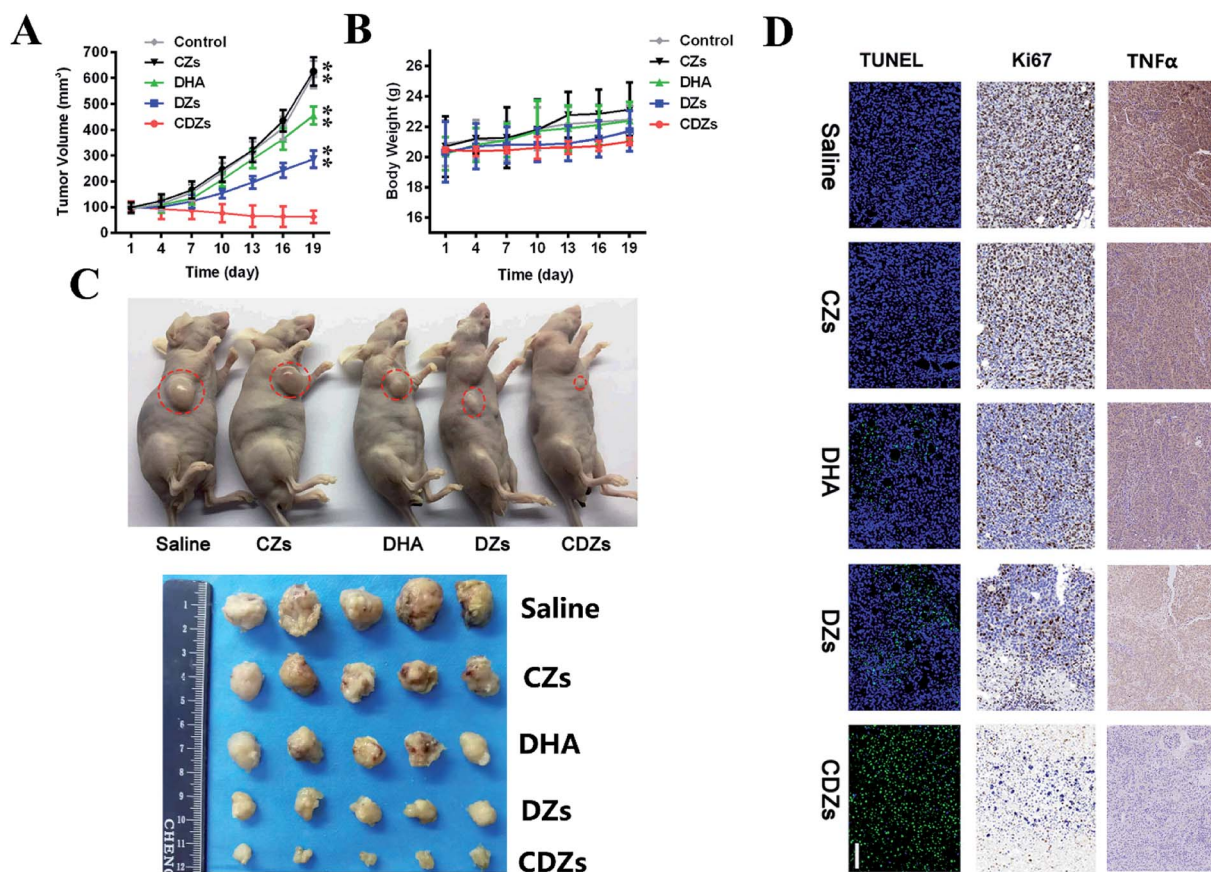

Fig. 7 *In vivo* anti-cancer effects of nanoparticles in hep G2 tumor-bearing nude mice. (A) Tumor growth profiles. (B) Body weight changes in 19 days after various treatments ($n = 5$). (C) Representative photos of tumor-bearing mice and tumor tissue at the end of the experiment. (D) Representative images (200×) of tumor tissues stained for Ki-67, terminal-deoxynucleoitidyl transferase mediated nick end labeling (TUNEL) staining, and TNFα of the tumor tissues. Scale bar = 100 μm. Statistical significance: *$p < 0.05$ and **$p < 0.01$.

that ZIF-8 nanoparticles could be used for delivering a high load of DHA along with its enhancer, Fe^{2+}. After treatment with CDZs, we observed a remarkable 90.8% reduction in the tumor volume when compared with the saline group. This increased efficacy may be attributed to cell membrane-induced homotypic accumulation of the nanoparticles and increased stability of the nanoparticles, thus minimizing drug loss. Changes in body weight of all the mice were recorded to evaluate systemic toxicity (Fig. 7B). Neither death nor significant difference in the body weight change was observed in the treated groups and the control

groups. The remarkable anti-tumor effect of CDZs was verified by visible reductions in the tumor size (Fig. 7A). Ki-67, TUNEL, and TNFα staining results are shown in Fig. 7D; the Ki-67 staining results revealed that the CDZs treatment inhibited the proliferation of tumor cells than the other groups more significantly. The mice treated with CZs without DHA exhibited a similar growth behavior as the saline group without significant anti-tumor effects and little cell apoptosis. After loading DHA in ZIF-8, cell apoptosis was significantly increased compared with CZs; when injected intravenously with CDZs, terminal-deoxynucleoitidyl
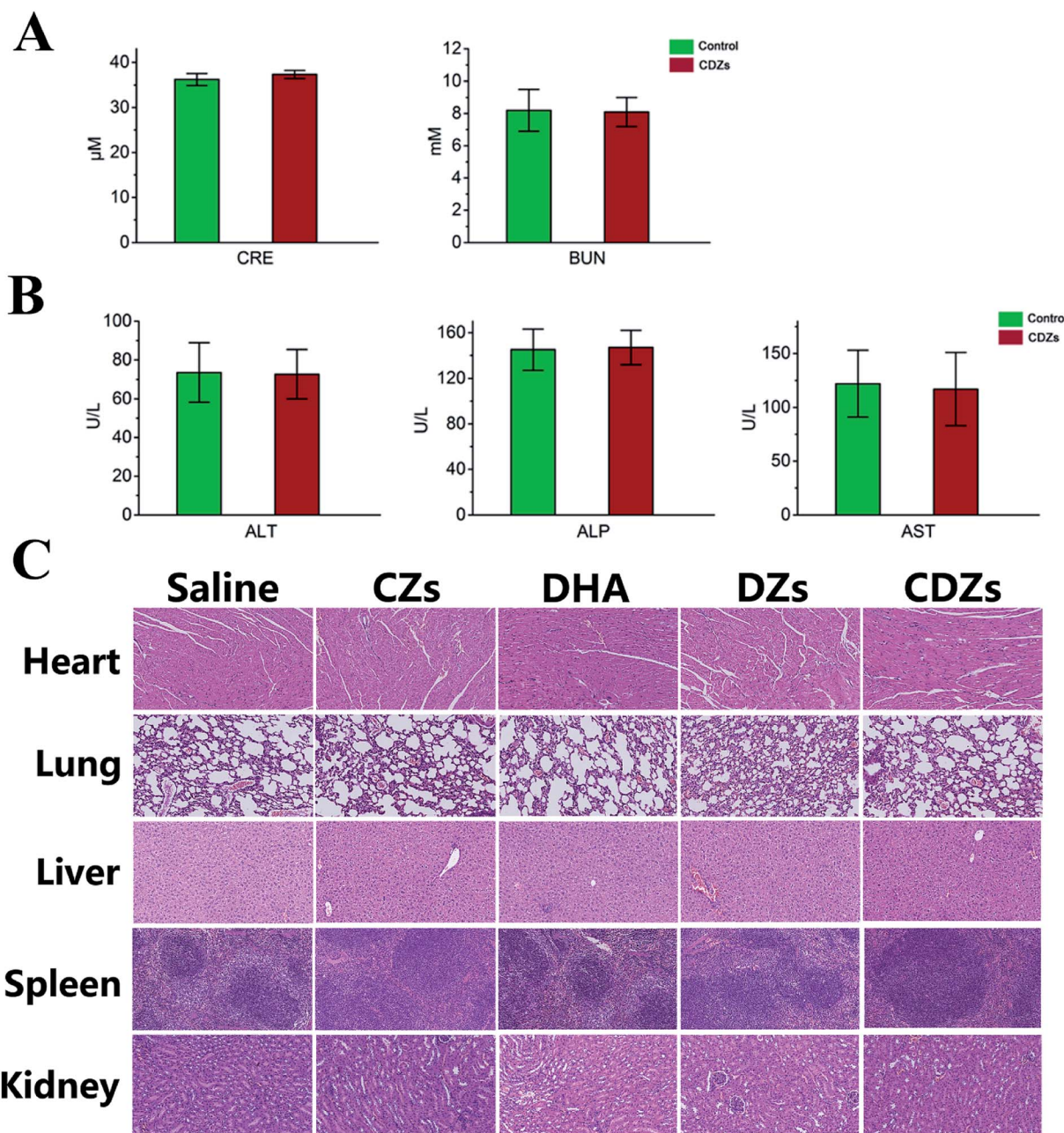

Fig. 8 *In vivo* toxicity assessment and blood biochemistry test. (A) Renal function (CRE, BUN) examination in the blood of BALB/c nude mice. (B) Liver function (AST, ALT, and ALP) examination in the blood of BALB/c nude mice ($n = 5$). (C) Histopathologic examination of the tissues including heart, liver, spleen, lungs, and kidney from BALB/c nude mice after intravenous administration of saline, CZs, DHA, DZs, and CDZs for 19 d. Scale bar = 100 μm.

transferase mediated nick end labeling (TUNEL) staining showed the strongest cell apoptosis with the highest green fluorescence distributed around the whole tumor tissues (Fig. 7D), which can be attribute to the cell membrane-induced homotypic accumulation of the nanoparticles, increased stability of nanoparticles minimizing drug loss, and significant anti-tumor effect of DHA, in accordance with tumor inhibition. The TNFα staining results suggested that the inflammatory response was weakest in the CDZs group. In all, these results confirmed that CDZs have potent anti-cancer activity *in vivo*.

In vivo toxicity assessment

Two kidney function indicators (CRE, creatinine and BUN, blood urea nitrogen) and three liver function indicators (AST, aspartate aminotransferase; ALP, alkaline phosphatase; ALT, alanine aminotransferase) were measured, and the results suggested that no distinct hepatic or renal toxicity was induced by these treatments (Fig. 8A and B). Furthermore, no obvious organ damage was observed in the hematoxylin and eosin (H&E)-stained sections (Fig. 8C). All systematic toxicity results pointed to good biocompatibility of CDZs.

Conclusion

In summary, we have designed a biomimetic nanomedicine consisting of a cancer cell membrane-derived shell encapsulating a dihydroartemisinin-loaded ZIF-8 core doped with ferrous ion. Benefiting from the homologous targeting of CCMs, this nanomedicine can actively target hep G2 cancer cells both *in vitro* and *in vivo*. The acid-sensitive ZIF-8 nanoparticle core exhibited high drug loading efficiency and controllable drug release. Combining the anti-malarial drug DHA and Fe^{2+} released from ZIF-8 nanoparticles resulted in a 90.8% reduction in tumor growth in a hep G2 subcutaneous tumor model. This was all achieved with virtually no damage to the main organs and no changes in the white blood cell and platelets levels, indicating superior biocompatibility. In brief, this system holds great promise as a therapy for hepatocellular carcinoma.

Conflicts of interest

There are no conflicts of interest to declare.

Acknowledgements

References

1 A. Ally, M. Balasundaram, R. Carlsen, E. Chuah, A. Clarke, N. Dhalla, R. A. Holt, S. J. Jones, D. Lee and Y. Ma, *Cell*, 2017, **169**, 1327–1341.

2 X. Zhang, H. L. H. Ng, A. Lu, C. Lin, L. Zhou, G. Lin, Y. Zhang, Z. Yang and H. Zhang, *Nanomedicine*, 2016, **12**, 853–869.

3 T. Chen, M. Li, R. Zhang and H. Wang, *J. Cell. Mol. Med.*, 2009, **13**, 1358–1370.

4 C. Qu, J. Ma, X. Liu, Y. Xue, J. Zheng, L. Liu, J. Liu, Z. Li, L. Zhang and Y. Liu, *Front. Cell. Neurosci.*, 2017, **11**, 310.

5 N. P. Singh and H. C. Lai, *Anticancer Res.*, 2004, **24**, 2277–2280.

6 Y. Li, H. Sui, C. Jiang, S. Li, Y. Han, P. Huang, X. Du, J. Du and Y. Bai, *Cell. Physiol. Biochem.*, 2018, **48**, 2035–2045.

7 H. Li, X. Li, X. Shi, Z. Li and Y. Sun, *Phytomedicine*, 2019, **56**, 215–228.

8 N. P. Singh and H. Lai, *Life Sci.*, 2001, **70**, 49–56.

9 J. Chen, Z. Guo, H.-B. Wang, J.-J. Zhou, W.-J. Zhang and Q.-W. Chen, *Biomaterials*, 2014, **35**, 6498–6507.

10 L. Liu, Y. Wei, S. Zhai, Q. Chen and D. Xing, *Biomaterials*, 2015, **62**, 35–46.

11 D. Wang, J. Zhou, R. Chen, R. Shi, G. Xia, S. Zhou, Z. Liu, N. Zhang, H. Wang and Z. Guo, *Biomaterials*, 2016, **107**, 88–101.

12 X. Gao, X. Hai, H. Baigude, W. Guan and Z. Liu, *Sci. Rep.*, 2016, **6**, 37705.

13 D. Chen, D. Yang, C. A. Dougherty, W. Lu, H. Wu, X. He, T. Cai, M. E. Van Dort, B. D. Ross and H. Hong, *ACS Nano*, 2017, **11**, 4315–4327.

14 C. Y. Sun, C. Qin, C. G. Wang, Z. M. Su, S. Wang, X. L. Wang, G. S. Yang, K. Z. Shao, Y. Q. Lan and E. B. Wang, *Adv. Mater.*, 2011, **23**, 5629–5632.

15 X. Gao, M. Zhai, W. Guan, J. Liu, Z. Liu and A. Damirin, *ACS Appl. Mater. Interfaces*, 2017, **9**, 3455–3462.

16 Z. Zou, S. Li, D. He, X. He, K. Wang, L. Li, X. Yang and H. Li, *J. Mater. Chem. B*, 2017, **5**, 2126–2132.

17 H. Zhang, W. Jiang, R. Liu, J. Zhang, D. Zhang, Z. Li and Y. Luan, *ACS Appl. Mater. Interfaces*, 2017, **9**, 19687–19697.

18 D. Hanahan and R. A. Weinberg, *Cell*, 2011, **144**, 646–674.

19 G. A. Rabinovich, D. Gabrilovich and E. M. Sotomayor, *Annu. Rev. Immunol.*, 2007, **25**, 267–296.

20 W. Huang, T. Zhang, X. Hu, Y. Wang and J. Wang, *Microchim. Acta*, 2018, **185**, 37.

21 S. R. MacEwan, D. J. Callahan and A. Chilkoti, *Nanomedicine*, 2010, **5**, 793–806.

22 W. Huang, T. Zhang, X. Hu, Y. Wang and J. Wang, *Microchimica Acta*, 2018, **185**, 37.

23 H. Y. Wang, S. F. Hung, H. Y. Chen, T. S. Chan, H. M. Chen and B. Liu, *J. Am. Chem. Soc.*, 2016, **138**, 36–39.

24 L. Chen, Y. Peng, H. Wang, Z. Gu and C. Duan, *Chem. Commun.*, 2014, **50**, 8651–8654.

25 R. H. Fang, C. M. Hu, B. T. Luk, W. Gao, J. A. Copp, Y. Tai, D. E. O'Connor and L. Zhang, *Nano Lett.*, 2014, **14**, 2181–2188.

26 M. He, J. Zhou, J. Chen, F. Zheng, D. Wang, R. Shi, Z. Guo, H. Wang and Q. Chen, *J. Mater. Chem. B*, 2015, **3**, 9033–9042.

27 R. Chen, J. Zhang, Y. Wang, X. Chen, J. A. Zapien and C.-S. Lee, *Nanoscale*, 2015, **7**, 17299–17305.

28 H. Zheng, Y. Zhang, L. Liu, W. Wan, P. Guo, A. M. Nyström and X. Zou, *J. Am. Chem. Soc.*, 2016, **138**, 962–968.

29 S. Wang, L. Shang, L. Li, Y. Yu, C. Chi, K. Wang, J. Zhang, R. Shi, H. Shen and G. I. Waterhouse, *Adv. Mater.*, 2016, **28**, 8379–8387.